The Iranian Journal of Mechanical Engineering Transactions of ISME
Journal homepage: https://jmee.isme.ir/
Vol. 25, No. 1, 2024, pp. 21-40

Research Paper

DOI: https://doi.org/10.30506/jmee.2024.2014704.1328

Viscoelastic Analysis of Malignant Breast Tumors using Fractional Derivative Model and in Vitro Test Data

Arisa Monshizadeh[*]
M.Sc. Student

Afsaneh Mojra[†]
Associate Professor

Examining the breast mechanical behavior helps with early diagnosis and successful treatment. Identification of tumor malignancy by evaluating its mechanical behavior can significantly facilitate early detection task. In the present study, using a precise viscoelastic model based on time-dependent tissue behavior, the breast mechanical behavior has been investigated to distinguish malignant from benign tumors. For this purpose, benign and malignant samples have been collected, and in vitro ramp-relaxation test has been performed. The Kelvin-Voight fractional derivative model has been fitted to experimental data with an accuracy of 0.97 and the model parameters have been well estimated. For malignant samples, the mean of elasticity, fluidity, and time constant are equal to 70MPa, 0.22, and 180s, respectively. It has been concluded that malignant and benign samples significantly differ in the value of viscoelastic parameters. The findings have been evaluated based on pathology images and results demonstrate a positive correlation between the mechanical characteristics and density of cancer cells. Furthermore, it emphasizes the importance of understanding this correlation in order to enhance the accuracy and effectiveness of breast cancer diagnosis by medical professionals.

Keywords: Breast cancer, Kelvin-Voigt fractional derivative model, Mechanical characterization, Relaxation, Viscoelasticity

1 Introduction

There is a high incidence of and mortality rate associated with breast cancer among women throughout the world [1-5].

[*]M.Sc., Student, Department of Mechanical Engineering, K. N. Toosi University of Technology, Tehran, Iran, monshizadeharisa@gmail.com
[†] Corresponding Author, Associate Professor, Department of Mechanical Engineering, K. N. Toosi University of Technology, Tehran, Iran, mojra@kntu.ac.ir

Received: 2023/10/30, Revised: 2024/01/24, Accepted: 2024/03/12

According to the latest statistics of the World Health Organization (WHO), breast cancer is the most common type of cancer in the world, with more than 2.26 million new cases and about 685000 deaths [6,7].

Generally, breast cancer is divided into non-invasive and invasive types. Non-invasive breast cancer is limited to the tissue ducts, while the invasive type breaks through the ducts and lobular walls and attacks the breast fat and connective tissues [8-10]. Ductal carcinoma in situ (DCIS) is the most prevalent type of non-invasive breast cancer that is limited to the ducts of the breast. The phrase "in situ" denotes cancer that has not metastasized from its original site of development, and invasive ductal carcinoma (IDC) is the most aggressive type. IDC originates in the milk ducts of the breast and infiltrates the duct wall and the adipose tissue of the breast and spreads to other areas of the body [9,11]. The most critical point for the best prognosis is to recognize cancer cells at the early stages. There are standard diagnostic methods, including mammography, ultrasound, and breast MRI (magnetic resonance imaging). However, these methods have limitations, which can be considered expensive, time-consuming, and inappropriate for young women [12,13].

In recent years, alternative methods have been proposed instead of common diagnostic modalities. Mechanical diagnosis based on the measurement of soft tissue mechanical behavior is a suitable alternative, and its potential has been explored by many researchers [14,15]. It has been shown that the cancerous tissues' mechanical properties have a correlation with their pathology and cancer progression [16]. Accordingly, the identification of mechanical properties of breast tissue has valuable applications in various medical fields, such as breast cancer diagnosis, preoperative surgical planning, and postoperative surgical outcome prediction [17,18].

Breast tissue has a complex structure that changes with the emergence of tumors [19]. The mechanical properties of the breast are a complex combination of elastic and viscous behaviors, and tissue deformation is controlled by both elastic and viscous components. The focus of many primary studies has been on the elastic properties, and healthy tissue was distinguished from the cancerous one by measuring the elastic modulus [15,19,20]. However, when subjected to an external load, breast tissue has a nonlinear and time-dependent response. To address the time dependence, viscoelastic material models are used [21,22]. Among various models, the Kelvin-Voigt fractional derivative (KVFD) model has been recently introduced with high accuracy in fitting the experimental mechanical test data. The KVFD can adequately describe the elastic behavior and time-dependent viscosity of soft matter with three model parameters. The viscoelastic properties of fluidity and elasticity, based on the Kelvin- Voigt fractional derivative (KVFD) model, are capable of distinguishing normal, benign, and malignant breast biopsy tissues. In addition, the histopathological characteristics can be understood by interpreting the parameters of this model. Therefore, the mechanical properties of breast cancer tissue can be studied using the KVFD model [21,23-26]. In research by Zhang et al. [23], the breast phantoms' mechanical properties were investigated using the ramp-hold relaxation test and the KVFD and double Maxwell-arm Wiechert (DMW) models to interpolate experimental data. In another study by Mojra and Hooman [11], some viscoelastic parameters were proposed to identify the mechanical behavior of IDC using a ramp-relaxation test. For this purpose, the generalized Maxwell model was employed. The correlation between viscoelastic parameters and tissue porosity and magnesium-to-calcium ratio was suggested as the tissue malignancy index.

As described, different models have been used to evaluate the breast tissue behavior and its mechanical properties because as cancer progresses, the loss of biomechanical homeostasis of cells leads to significant changes in the mechanical phenotypes of cells and tissues [21]. However, the lack of accurate material models has been the disadvantage of most related studies. In contrast, in some limited studies, although the material model has been improved,

there is still grave concern about using natural biological tissue samples. Accordingly, in the present study, biopsied and natural cancerous samples are used, and mechanical testing is performed. The KVFD model is fitted to the computerized test data to evaluate the mechanical behavior of breast cancer tissue.
In the following, section 2 presents the methodology, including the biological sample preparation, the experimental test, and the material model. In section 3, the model validation and the results are analyzed and discussed. Finally, in section 4, all the conclusions are provided.

2 Material and methods

In this research, actual biological samples of cancerous breast tissue are examined, and a mechanical test is performed to characterize their viscoelastic response. In this regard, this section presents the steps taken for sample preparation and their specifications. Then, the procedure of mechanical testing is elaborated. Eventually, the governing equations of the KVFD model and the fitting of experimental data to the numerical model are provided.

2.1 Sample preparation

Biopsied tissue samples from human breast masses were obtained from Ayatollah Kashani Hospital, Tehran. The specimens were stored in histology containers biopsy pots containing 10% formalin solution at 25°C. The strong structure of these containers can protect the tissue against difficult transportation conditions and years of storage [27].
Based on the pathology reports, the samples were divided into two groups: benign and malignant masses. One example of a malignant sample (sample #2) and one example of a benign legion (sample #3) are shown in Figure (1). The age of donors, the mass types, and the information obtained from the pathology reports and dimensions of each sample are provided in Table (1).

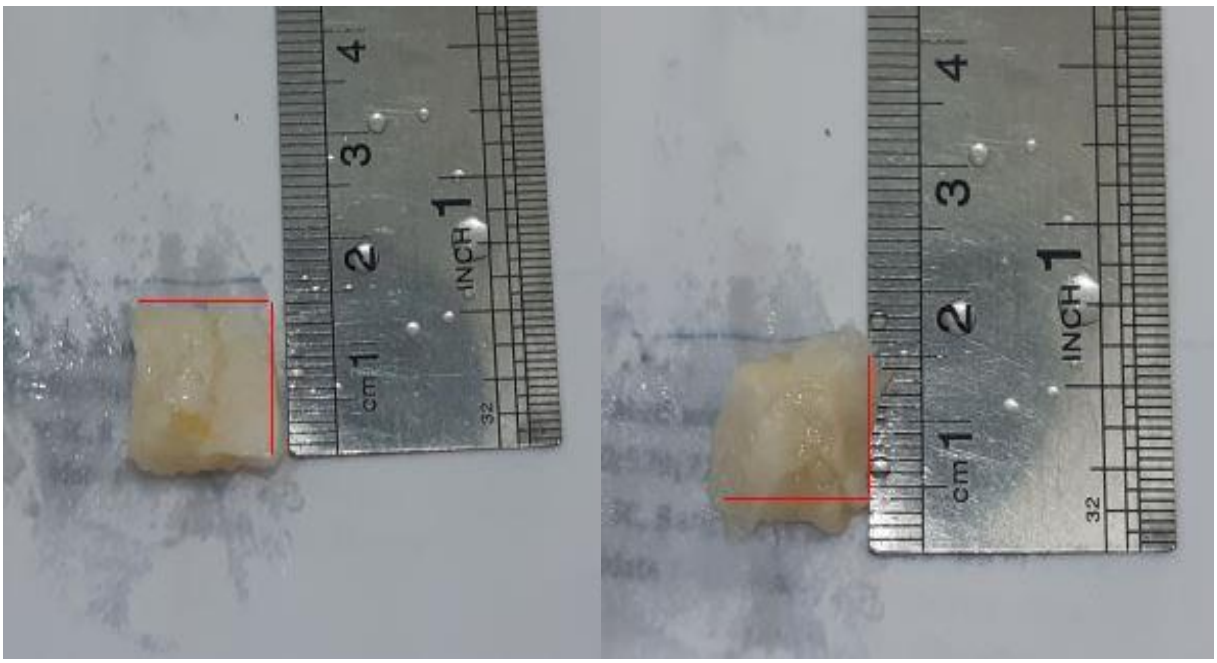

(**a**) (**b**)

Figure 1 (**a**) One example of a malignant sample (sample #2) and (**b**) one example of a benign legion (sample #3); the samples are cut into rectangular cube shapes to be placed between the plates of the measuring mechanical testing device, the dimensions are obtained using the Digitizer software, and the scale is shown.

Table 1 Age of donors, descriptions of pathology reports, and dimensions of each biological specimen; h_0 is the initial height, and A is the cross-section of the samples. Three of the samples are benign masses, and the rest are malignant masses. Sample #3 is large enough to be divided into two parts (samples #3-1 and #3-2) to check the results' consistency.

Sample No.	Age	h_0 (10^{-3} m)	A ($\times 10^{-6}$ m^2)	Pathology description
#1	40-50	5.39	11.0×9.25	Benign tumor: Fibrocystic
#2	40-50	4.40	15.00×14.12	Cancerous and malignant
#3-1	25-35	3.88	13.28×11.0	Benign tumor: Gynecomastia
#3-2	25-35	3.85	13.20×11.0	Benign tumor: Gynecomastia
#4	20-30	4.53	13.50×7.73	Benign tumor: Fibroadenoma
#5	45	6.90	21.0×15.0	Malignant and invasive: Ductal carcinoma
#6	48	7.00	21.0×19.0	Malignant and invasive: Ductal carcinoma

2.2 Ramp-relaxation test procedure

In this research, experimental data was collected using the ramp-relaxation test. This test is suitable for evaluating the elastic behavior of the tissue during the ramp phase. Meanwhile, it can be used to assess the viscous behavior during the hold phase. The samples were cut into rectangular cube shapes. Each piece was placed between two movable and fixed flat plates of the mechanical testing device. Before the test, a slight pressure was applied to the upper surface of the samples by moving the plate at a deficient speed so that the two surfaces of the piece became utterly parallel. Then, the force was applied to the sample by the moving plate until the thickness of the sample was reduced by 1 mm. At this time, the force was removed. The loading period was 180 seconds, and the speed of the moving plate was $0.667\,\frac{mm}{s}$ and $1\,\frac{mm}{s}$ in the ramp phase.

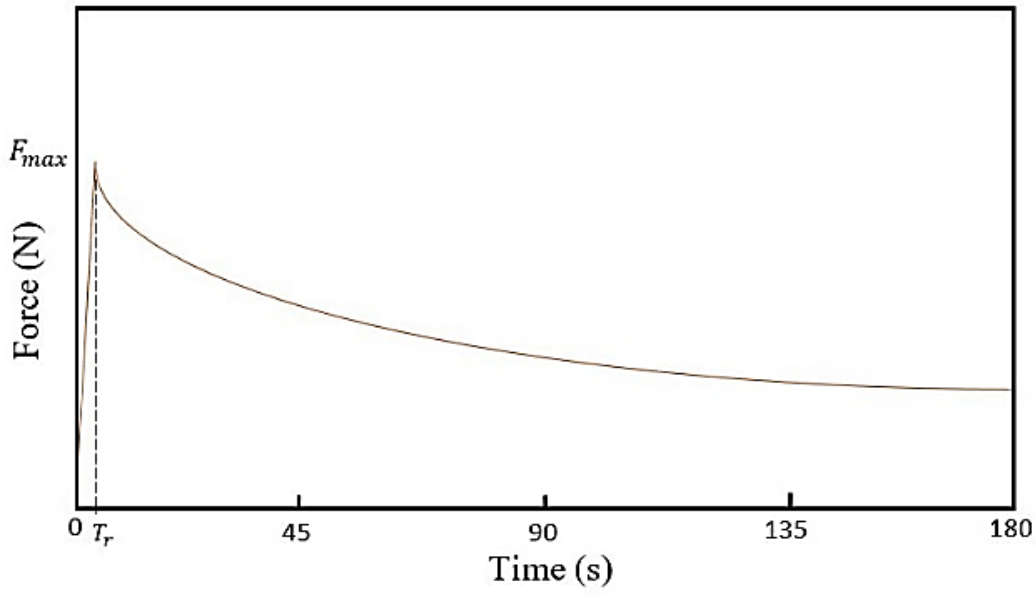

Figure 2 Ramp-hold diagram of testing procedure; the test duration is 180 seconds. T_r is the ramp time when the maximum force is applied to the specimen, and the tissue thickness reduces by 1mm.

The device provides hold phase data that shows how much force has been removed from the tissue since the ramp time, so at the beginning of the test, when the force is applied to the sample to reduce its thickness by 1 mm, it should be noted how much the applied force increases. The increased maximum force gives the maximum ramp force. The force data obtained from the device in the hold phase is added to the maximum force. The time data in the hold phase is given in the same way as the ramp data. Figure (2) represents a schematic of the ramp-hold diagram. As seen, T_r is the ramp time at which the maximum force is applied to the specimen. The loading force and ramp time for the samples are given in Table (2).
The device used for the experiments is STM-1 (SANTAM universal testing machine, Iran), which is shown in Figure (3). This device has a load cell with a capacity of 25 kg. This load cell belongs to class C3, and its model is H3-C3-25Kg-3B D55. This device has two movable and fixed plates whose diameter is 7 cm.

Table 2 The ramp time and maximum force in the ramp phase for different specimens

Sample No.	Maximum force (N)	T_r (min)
#1	0.66	0.0003
#2	24.7	0.0003
#3-1	17.57	0.0003
#3-2	18.18	0.0003
#4	27.15	0.0005
#5	0.68	0.0003
#6	0.76	0.0003

Figure 3 Device for the compression test (STM-1); the upper and lower plates are moving and fixed, respectively. The specimen is located on the fixed plate, and a uniaxial compression is applied to the sample with a controlled velocity.

2.3 Kelvin-Voigt Fractional Derivative (KVFD) viscoelastic model

The time-dependent relaxation behavior of breast tissue is described using the Kelvin-Voigt fractional derivative (KVFD) model. Due to its high flexibility, this model can explain the material properties by three distinct parameters, including the elasticity (E_0), a time constant (τ), and the derivative order (α) [28,29]. The KVFD model comprises a damper with a fractional element representing the tissue viscosity and a spring representing the elastic behavior [23,30,31]. The constitutive equation for strain $\varepsilon(t)$ and stress $\sigma(t)$ for the KVFD model is defined as Eq. (1):

$$\sigma(t) = E_0\varepsilon(t) + \eta\frac{d^\alpha\varepsilon(t)}{dt^\alpha} \tag{1}$$

Where η is defined as:

$$\eta = E_0\,\tau^\alpha \tag{2}$$

Here, η represents a viscous coefficient with time constant $\tau(s)$, and E_0 defines the elastic modulus (Pa). α expresses a unitless actual number between (0,1), and indicates the derivative order [32]. According to the relaxation modulus, G, of the material, which is time-dependent, the stress σ from the applied strain ε is calculated by the Boltzmann superposition integral [23]:

$$\sigma(t) = \int_{-\infty}^{t} G(t-\tau)\frac{d\varepsilon(\tau)}{d\tau}d\tau \tag{3}$$

The Laplace transform of Eqs. (1) and (3) gives [32]:

$$\sigma(s) = E_0\varepsilon(s) + E_0\tau^\alpha s^\alpha\varepsilon(s) = sG(s)\varepsilon(s) \tag{4}$$

It is obtained from Eq. (4) [32]:

$$G(s) = \frac{(E_0 + E_0(s\tau)^\alpha)}{s} \tag{5}$$

The current state of stress/strain depends on the past deformations due to the viscoelastic material's memory. [32]. $G(s)$ is obtained by the Laplace transformation of the above two equations and putting them equal, and then the inverse Laplace is taken from it to get $G(t)$.
The relaxation modulus in terms of time for the KVFD model will be as follows [23,32]:

$$G(t) = E_0 + \eta\frac{t^{-\alpha}}{\Gamma(1-\alpha)} = E_0\left[1 + \frac{\left(\frac{t}{\tau}\right)^{-\alpha}}{\Gamma(1-\alpha)}\right] \tag{6}$$

Where $\Gamma(z) = \int_0^\infty e^{-t}t^{z-1}dt$ is the Gamma function. The relaxation force response is obtained using the Boltzmann integral expression [23].

$$P(t) = \frac{8\sqrt{R}}{3}\int_0^t G(t-\tau)\frac{dh^{3/2}(\tau)}{d\tau}d\tau \tag{7}$$

Where $h(t)$ shows the indenter displacement (the moving plate) into the sample, $P(t)$ represents the force, and R is the indenter radius. It is obtained from Eqs. (6) and (7):

$$P_r(t) = \frac{8\sqrt{R}}{3}\int_0^t \left(E_0 + \eta\frac{(t-\tau)^{-\alpha}}{\Gamma(1-\alpha)}\right)\frac{dh^{3/2}(\tau)}{d\tau}d\tau \tag{8}$$

The ramp-hold displacement condition can be defined by:

$$h(t) = \begin{cases} kt, & 0 \le t \le T_r \\ h_{max} = kT_r, & t \ge T_r \end{cases} \tag{9}$$

Where k is the indenter speed and T_r is the ramp phase duration [23]. By combining Eqs. (8) and (9), the response of the relaxation force is modified as follows:

$$P_r(t) = \frac{8\sqrt{R}}{3}\int_0^t \left(E_0 + \eta\frac{(t-\tau)^{-\alpha}}{\Gamma(1-\alpha)}\right)\cdot\frac{3}{2}\,k^{\frac{3}{2}}\tau^{\frac{1}{2}}\,d\tau \tag{10}$$

(1) By defining $\xi = \frac{\tau}{t}$: $(0 \le t \le T_r)$

$$\begin{aligned}\int_0^t (t-\tau)^{\beta}\,\tau^{\frac{1}{2}}\,d\tau &= \int_0^1 t^{\beta}(1-\xi)^{\beta}\,t^{\frac{1}{2}}\xi^{\frac{1}{2}}\,t\,d\xi = t^{\frac{3}{2}+\beta}\int_0^1 \xi^{\frac{1}{2}}(1-\xi)^{\beta}d\xi \\ &= t^{\frac{3}{2}+\beta}B\left(\frac{3}{2},\beta+1\right)\end{aligned} \tag{11}$$

Where $(x,y) = \int_0^1 t^{x-1}(1-t)^{y-1}dt$, x > 0 and y > 0 defines the beta function. Then, from Eqs. (10) and (11), and by placing $\beta = -\alpha$, $P_r(t)$ would become:

$$\begin{aligned}P_r(t) &= 4\sqrt{R}k^{\frac{3}{2}}\left(\frac{2}{3}E_0t^{\frac{3}{2}} + \frac{\eta}{\Gamma(1-\alpha)}t^{\frac{3}{2}-\alpha}B\left(\frac{3}{2},1-\alpha\right)\right) \\ &= 4\sqrt{R}k^{\frac{3}{2}}E_0t^{\frac{3}{2}}\left[\frac{2}{3} + \frac{1}{\Gamma(1-\alpha)}\left(\frac{t}{\tau}\right)^{-\alpha}B\left(\frac{3}{2},1-\alpha\right)\right]\end{aligned} \tag{12}$$

(2) By defining $\xi = \frac{\tau}{T_r}$: $(t \ge T_r)$

$$\int_0^{T_r}(t-\tau)^{\beta}\,\tau^{\frac{1}{2}}\,d\tau = \int_0^1 t^{\beta}\left(1-\xi\frac{T_r}{t}\right)^{\beta}\,t^{\frac{3}{2}}\left(\xi\frac{T_r}{t}\right)^{\frac{1}{2}}\,d\left(\xi\frac{T_r}{t}\right) \tag{13}$$

Letting $\zeta = \xi\frac{T_r}{t}$:

$$\int_0^{T_r}(t-\tau)^{\beta}\,\tau^{\frac{1}{2}}\,d\tau = \int_0^{\frac{T_r}{t}} t^{\frac{3}{2}+\beta}\,\zeta^{\frac{1}{2}}\,(1-\zeta)^{\beta}\,d\zeta = t^{\frac{3}{2}+\beta}\,B\left(\frac{T_r}{t};\frac{3}{2},\beta+1\right) \tag{14}$$

Where $B(a: x, y) = \int_0^a t^{x-1}(1-t)^{y-1}dt$, $\alpha \in [0,1]$ defines the incomplete Beta function [23]. From the combination of two Eqs. (10) and (14) and substituting $\eta = E_0\tau^\alpha$, $P_r(t)$ is obtained as follows:

$$P_r(t) = 4\sqrt{R}k^{\frac{3}{2}}\left(\frac{2}{3}E_0T_r^{\frac{3}{2}} + \frac{\eta}{\Gamma(1-\alpha)}t^{\frac{3}{2}-\alpha}B\left(\frac{T_r}{t};\frac{3}{2},1-\alpha\right)\right)$$
$$= 4\sqrt{R}k^{\frac{3}{2}}E_0T_r^{\frac{3}{2}}\left[\frac{2}{3} + \frac{1}{\Gamma(1-\alpha)}\left(\frac{t}{T_r}\right)^{\frac{3}{2}}\left(\frac{t}{\tau}\right)^{-\alpha}B\left(\frac{T_r}{t};\frac{3}{2},1-\alpha\right)\right] \quad (15)$$

Employing Eqs. (12) and (15), the ramp-hold relaxation solution is:

$$P_r(t) = \begin{cases} 4\sqrt{R}k^{3/2}E_0t^{3/2}\left[\frac{2}{3} + \frac{(t/\tau)^{-\alpha}}{\Gamma(1-\alpha)}B\left(\frac{3}{2},1-\alpha\right)\right], & 0 \le t \le T_r \\ 4\sqrt{R}k^{3/2}E_0T_r^{3/2}\left[\frac{2}{3} + \frac{\left(\frac{t}{T_r}\right)^{\frac{3}{2}}\left(\frac{t}{\tau}\right)^{-\alpha}}{\Gamma(1-\alpha)}B\left(\frac{T_r}{t};\frac{3}{2}.1-\alpha\right)\right], & t \ge T_r \end{cases} \quad (16)$$

In Eq. (16), $B(x,y) = \int_0^1 t^{x-1}(1-t)^{y-1}dt$ shows the complete beta function.
Also, $B(a: x, y) = \int_0^a t^{x-1}(1-t)^{y-1}dt$, $a \in [0,1]$ shows the incomplete beta function, and T_r is the ramp time [23].
To find the three parameters, Eq. (16) should be fitted to the experimental data using a developed MATLAB code. An overview of the developed MATLAB code is shown in Figure (4).

3 Results and discussion

In this section, first, the developed MATLAB code and the numerical model are validated. Following this, the results of testing the biological specimens and the associated mechanical parameters related to the KVFD model are presented and discussed. Finally, the obtained mechanical parameters are evaluated based on the pathology images.

3.1 Validation

The validation is carried out by comparing the present study results with the results of Zhang et al. [23]. In [23], the mechanical properties of tissue-mimicking phantoms were investigated using a ramp-hold relaxation test and the KVFD and double Maxwell-arm Wiechert (DMW) models.
The breast phantoms were made of gel powder and different percentages of skin cream.
Three parameters (E_0, α, τ) of the KVFD model for a 5%Gel15%Cream sample were obtained. Figure (5) shows the curve fitting of the experimental data by Zhang et al. [23] by the numerical model of the present study. It can be seen that there is a good conformity between the results. Additionally, the viscoelastic parameters from Zhang et al. [23] and the present study are reported in Table (3). A comparison indicates the validity of our developed code.

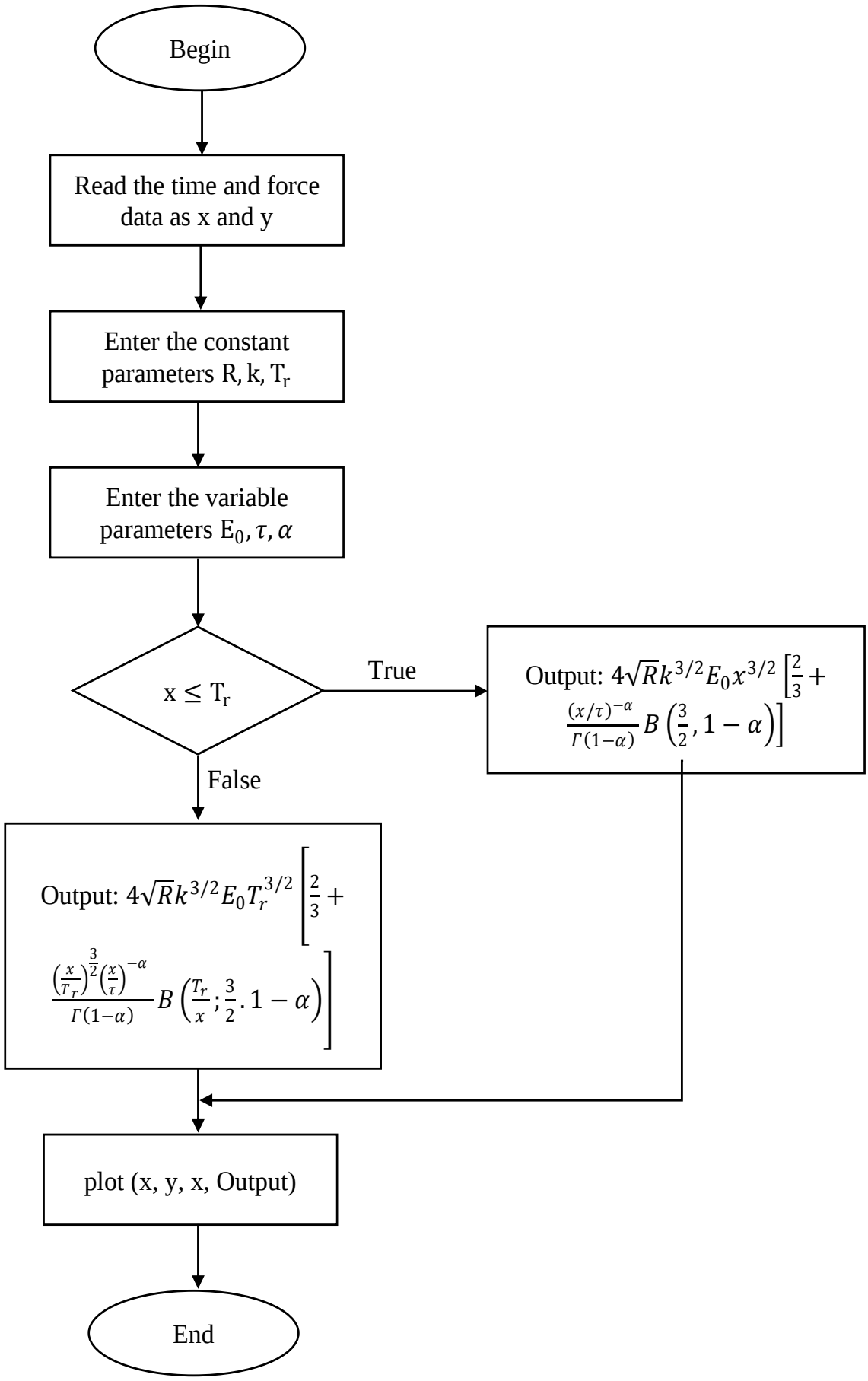

Figure 4 MATLAB code diagram for fitting the material model to the experimental data of force versus time

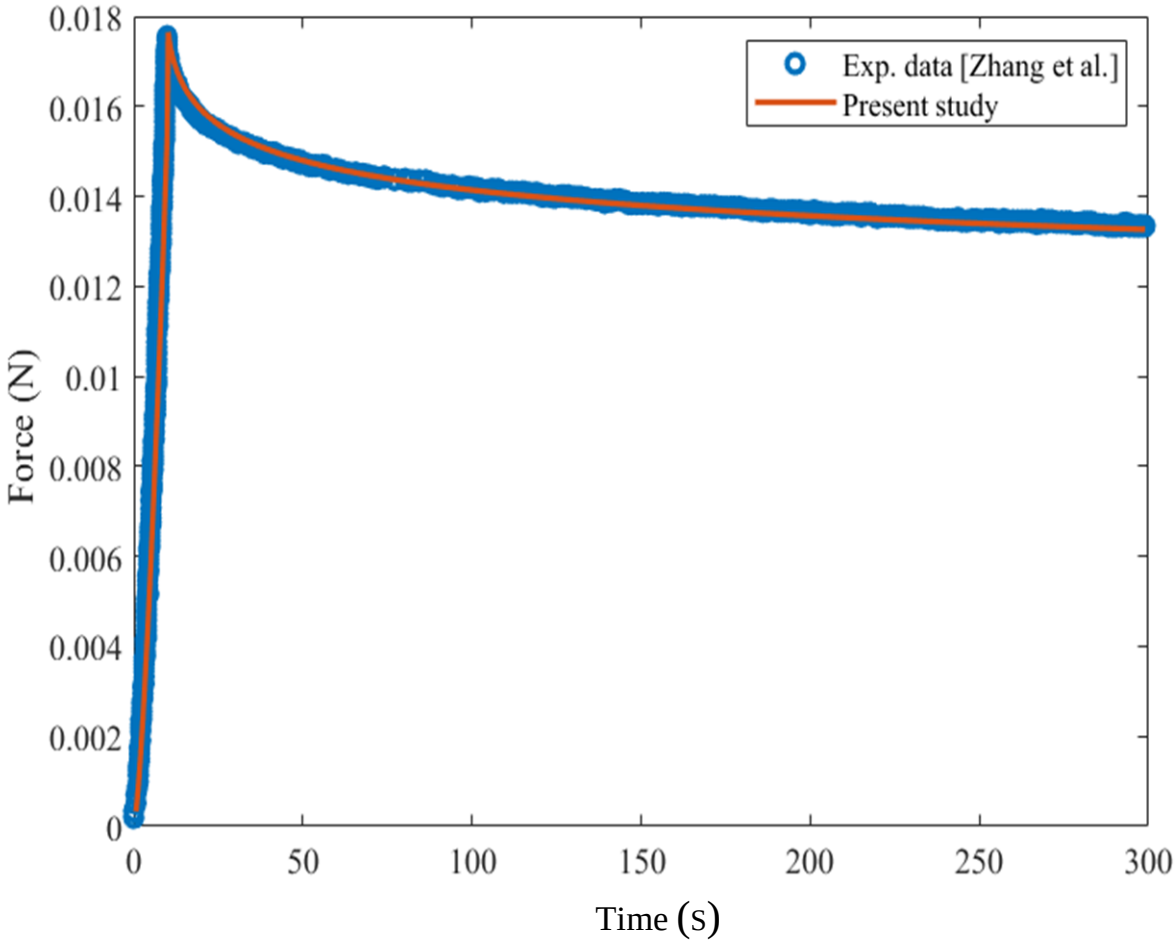

Figure 5 Curve fitting of the experimental data by Zhang et al. [23] by the numerical model of the present study. The red line shows the KVFD model function for the present study, and the blue circles show the experimental force-relaxation curve from [23].

Table 3 Comparison of KVFD model parameters between the Present study and Zhang's article [23]. E_0, τ, and α express the elastic modulus, time constant, and the fluidity, respectively. The fitting quality is evaluated based on the R^2-squared criterion.

Article	$E_0\ (MPa)$	α	$\tau\ (s)$	R^2
Zhang et al. [23]	2021.3	0.135	30.192	0.988
Present study	2020.5	0.133	30.0	0.98

3.2 Benign and malignant differentiation

The specimens were examined by a ramp-hold test according to Figure (2) and Table (2). According to pathology reports in Table (1), the specimens will be evaluated as being benign or malignant. Figure (6) plots the graph of the force versus time experimental data for various breast tissue specimens, benign and malignant.

Using the developed MATLAB code, the KVFD model is fitted to the experimental data, as shown in Figure (7). Inspection of the fitting quality indicates that in the ramp phase, a perfect fitting is observed. The quality deteriorated at the beginning of the relaxation phase for some specimens, although the quality improved after a few seconds. By the end of the relaxation period, the tissue response is well captured by the KVFD material model.

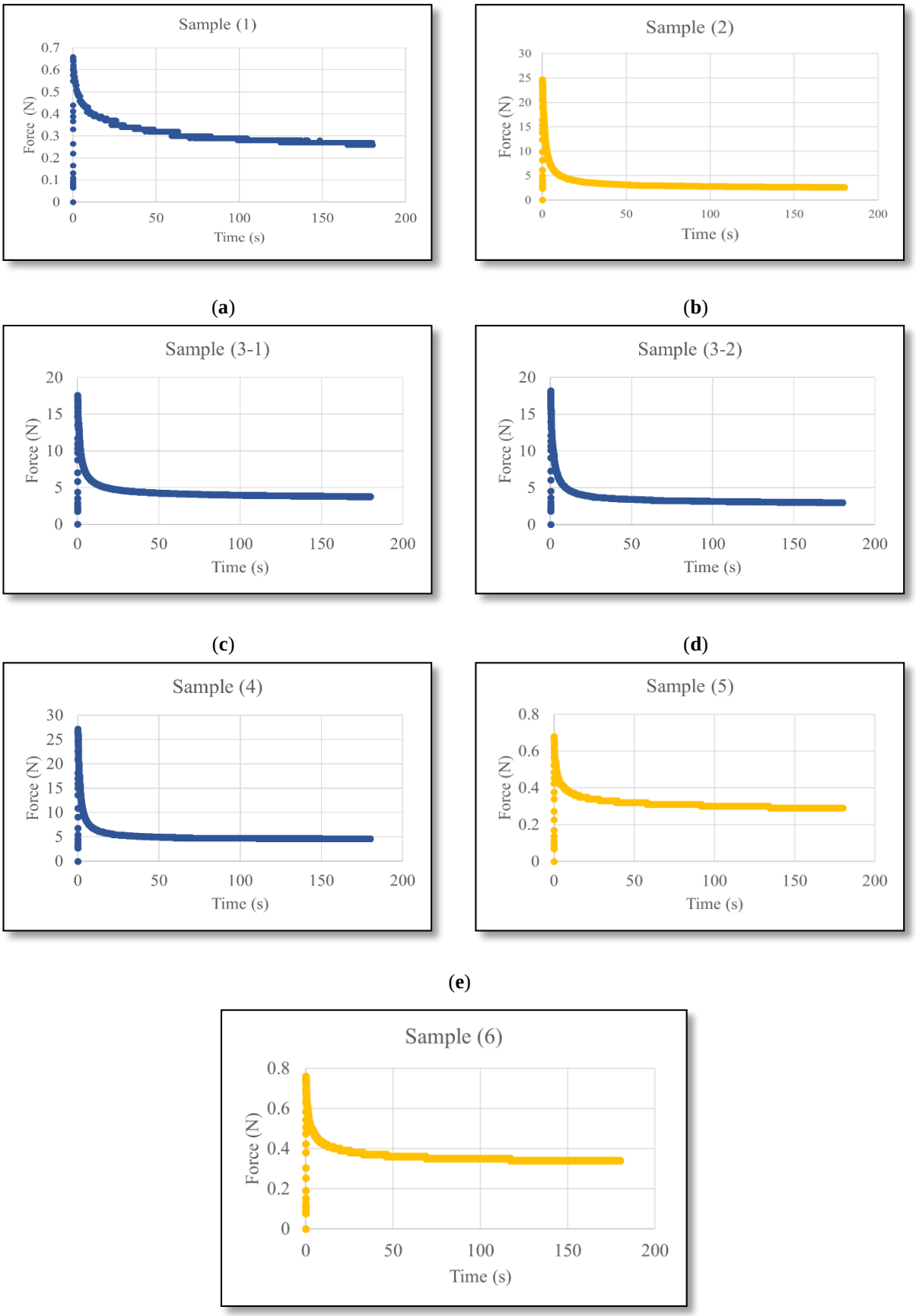

Figure 6 The graph of the force versus time experimental data for various breast tissue specimens: (**a**) to (**g**) belong to samples #1 to #6 .The diagram of benign masses (sample #1, #3-1, #3-2, #4) and malignant masses (sample #2, #5, #6) is plotted with blue and yellow colors, respectively.

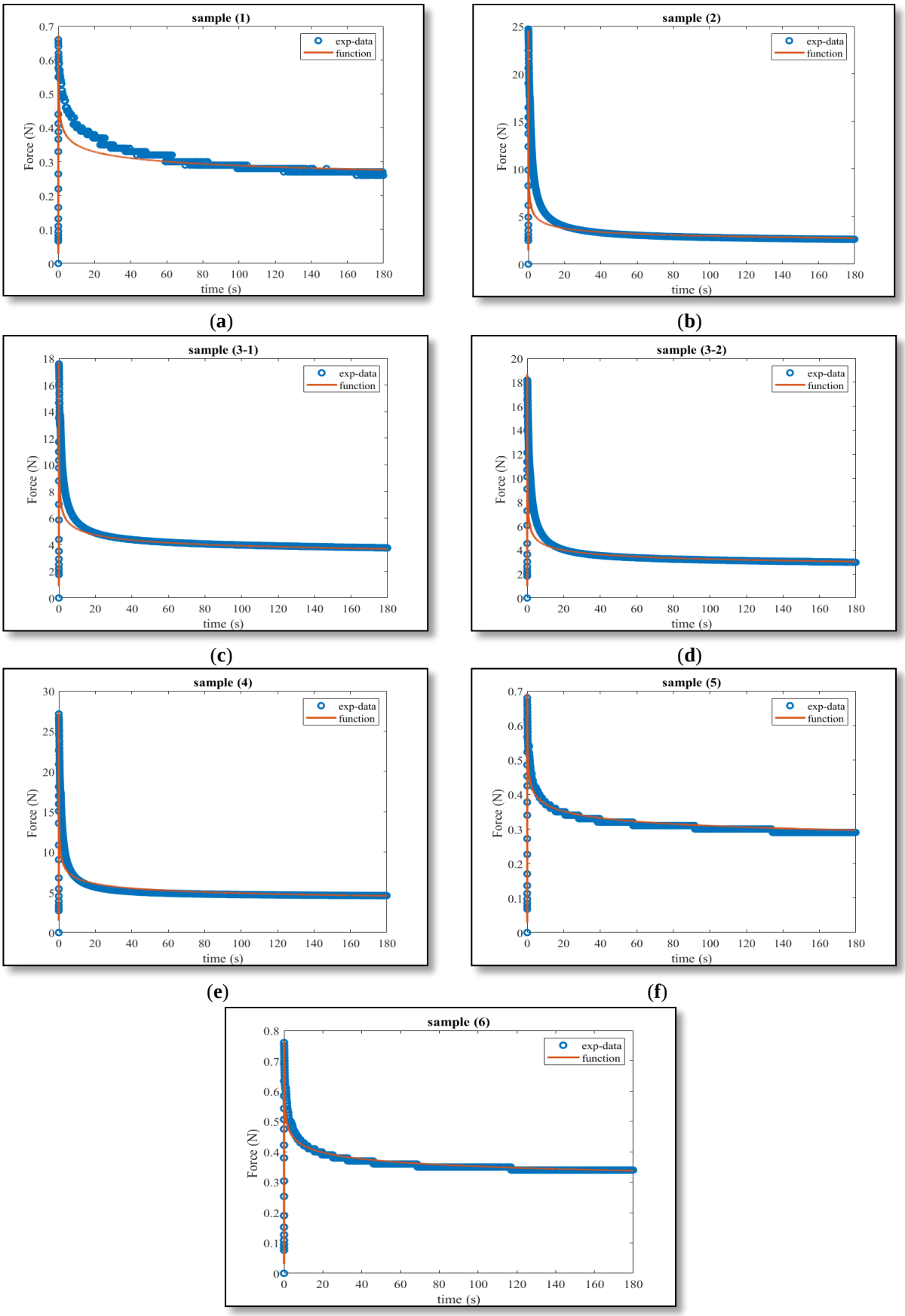

Figure 7 The graph of the force versus time experimental data and the fitted curve by the KVFD model. (**a**) to (**g**) belong to samples #1 to #6. The red line shows the KVFD model function, and the blue circles show the experimental ramp-relaxation curve.

The quality of fitting is further investigated by the R-squared values. Additionally, the three viscoelastic parameters, including the elasticity, the time constant, and the fluidity in the KVFD model, are reported for all samples in Table (4). The closer the coefficient of determination R^2 is to 1, the better the fitted model is. So, according to the R^2 value, the best fitting belongs to sample # 5 with $R^2 = 0.9759$.

Table 4 Estimated parameters by the KVFD model for samples #1 to #6. E_0 shows the elasticity, τ expresses the time constant, and α is the fluidity; the fitting quality is evaluated based on the R-squared values.

Sample No.	E_0 (MPa)	α	τ (s)	R^2
#1	6.4	0.15	140	0.95
#2	70.0	0.22	180	0.86
#3-1	95.0	0.225	120	0.90
#3-2	81.0	0.228	120	0.87
#4	56.0	0.257	140	0.85
#5	3.8	0.161	140	0.97
#6	4.3	0.165	140	0.96

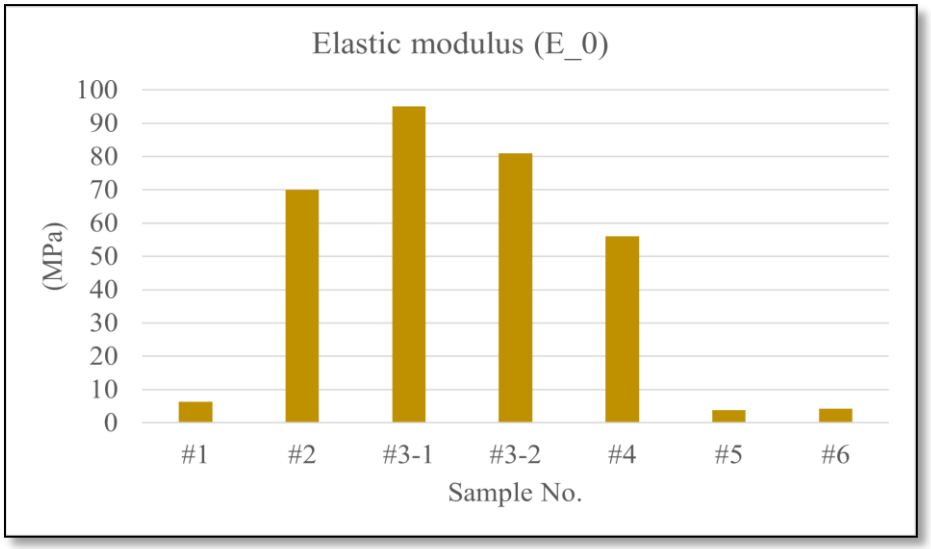

(**a**)

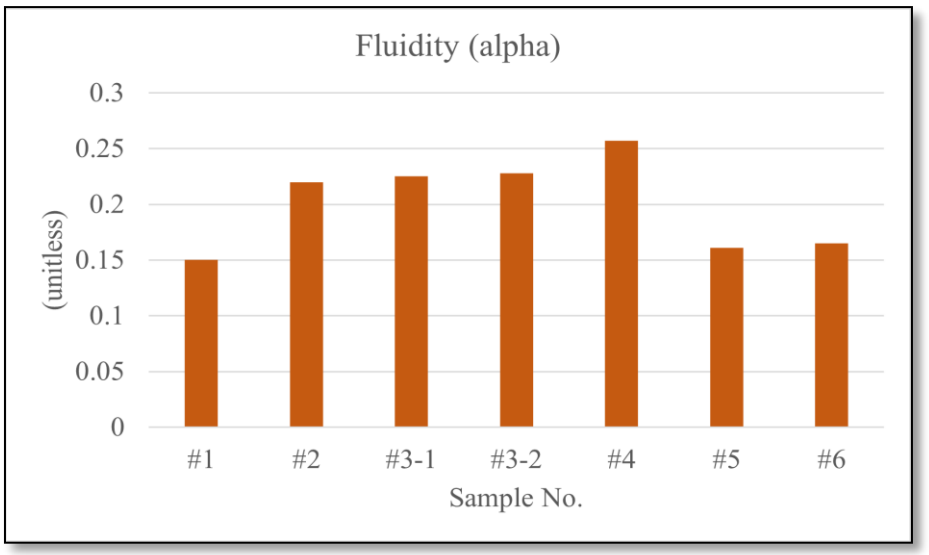

(**b**)

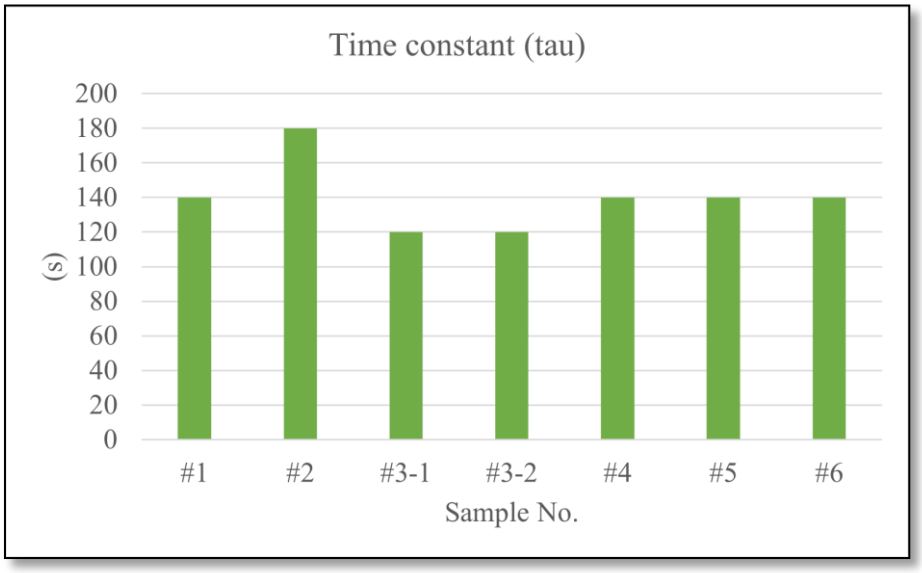

(**c**)

Figure 8 Estimated parameters by the KVFD model for samples #1 to #6: (**a**) modulus of elasticity (E_0), (**b**) the fluidity (α), (**c**) the time constant (τ).

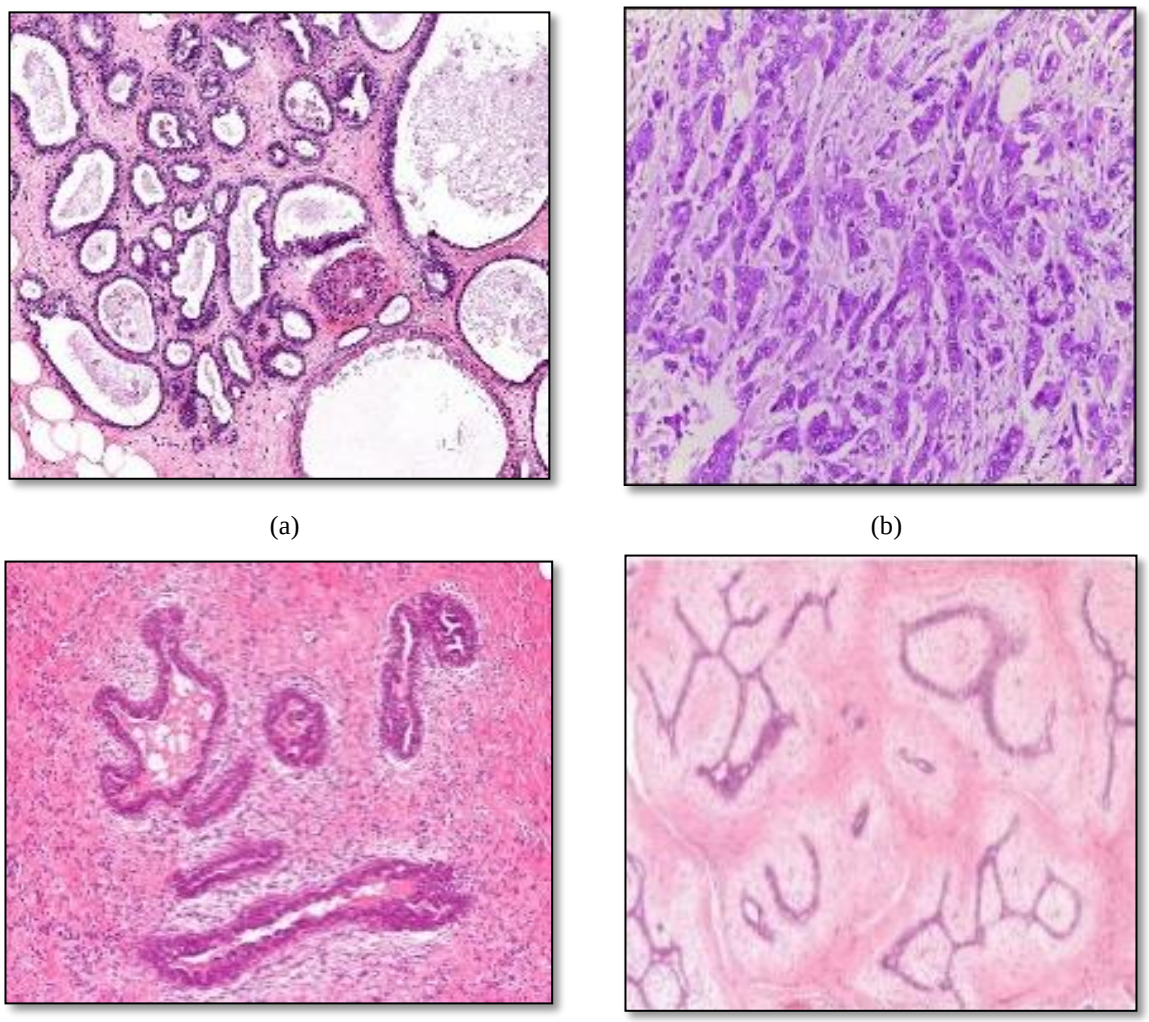

(a) (b)

(**c**) (**d**)

Figure 9 Pathology lab photos of the specimens: (**a**) to (**d**) represent samples #1 to #4, respectively. Connective tissues and differences in the cell density for each sample are displayed, and ductal and lobular cells can be seen in the pathology images.

Figure (8) shows the three parameters of the KVFD model for all samples as a bar chart.
To evaluate the benign and malignancy of tumor samples based on the mechanical response, samples #1 and #4 (benign) and #2 (malignant) are compared. As seen in Table (4) and Figure (8), the parameter E_0 in sample #2 is higher than the corresponding value for samples #1 and #4. It can be inferred that the elastic modulus of a malignant mass is higher than that of a benign mass. This deduction can be related to the difference in the cell type and density. Additionally, the fluidity parameter (α) is higher in sample #4 than in sample #2, and it is higher in sample #2 than in sample #1. From the results, it is concluded that the value of this parameter is smaller for malignant masses than benign masses. Further investigation is performed by inspecting the pathology lab images of the samples, which are given in Figure (9).
According to the pathologic data (Figure 9a), sample #1 is fibrocystic. The cysts cause a space in the tissue and reduce the tissue resistance to the force, resulting in a relatively small E_0.
In sample #2, as seen in Figure (9b), the density of cells is very high, and the specimen is a highly aggressive type, which causes the tissue to show excellent resistance to the force, and the value of E_0 increases.
Sample #4 is one of the types of fibroadenomas, and these types of tumors have severe fibrosis that creates stiffer tissue. As shown in Figure (9d), the ducts expand within the tissue, which is composed of benign cells. Since the fibrosis volume is more than the ducts, enhancements are observed in the tissue resistance and the value of E_0.
For sample number 3, two samples (3-1 and 3-2) were biopsied from different areas of a patient's breast to evaluate the effect of the difference in the biopsy area on the tissue's mechanical properties. The two samples were examined based on the KVFD model. Figure (9c) shows the pathology image of sample #3. As seen in Table (4), there are insignificant differences in the estimated parameters of the KVFD model, which verifies the reliability of the analysis. Slight differences in the value of E_0 can be caused by the cell density variation in different areas of the breast tissue.

3.3 Impact of loading rate on malignant tumor response

To study the impact of loading rate on the viscoelastic response, the loading velocity is varied for malignant specimens. As previously mentioned in section (2.2), the speed of the moving plate was $0.667\,\frac{mm}{s}$ for sample #2, which was increased to $1\,\frac{mm}{s}$ for samples #5 and #6. Table (5) reports the KVFD model parameters for sample #2 compared with the corresponding values for samples #5 and #6.

Table 5 Estimated parameters by the KVFD model for malignant samples #2, #5, and #6. E_0, τ, and α express the elastic modulus, time constant, and the fluidity, respectively

Sample No.	E_0 (MPa)	α	τ (s)
#2	70	0.220	180
#5	3.8	0.161	140
#6	4.3	0.165	140

As seen in Table (5), the elastic modulus reduces with an increase in the loading rate. There is a possibility that this finding is related to the differences in tissue structure that occur during compression. At lower loading rates, the tissue encounters higher deformation, which results in a more compact form and increased stiffness. Further inspection of Figure (10) reveals that in sample #5, the connective tissue is more expanded than sample #6, which creates a lot of space and reduces the tissue's resistance against the applied force.

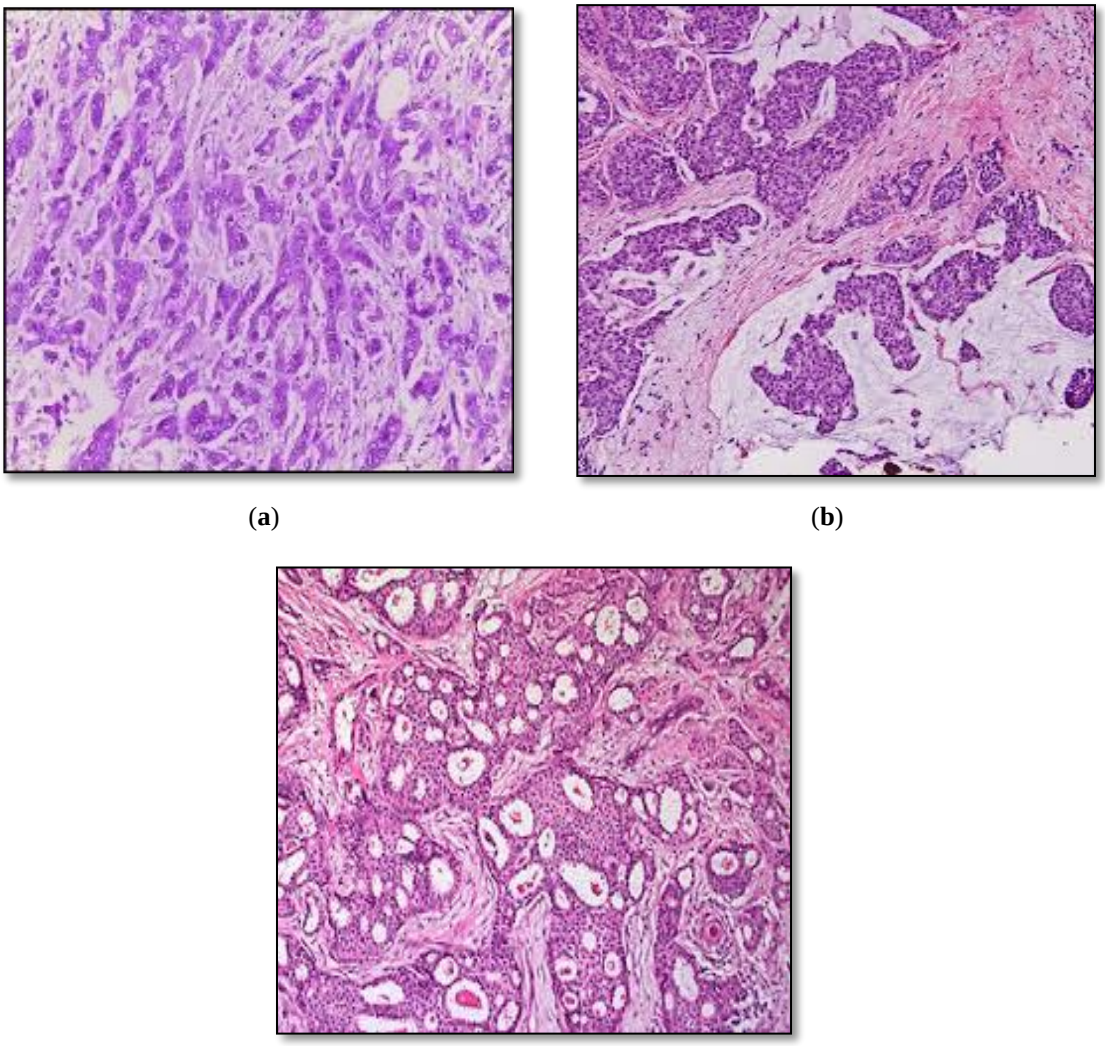

(**a**) (**b**)

(**c**)

Figure 10 The pathology lab images of malignant samples: (**a**) to (**c**) belong to samples #2, #5, and #6, respectively.

4 Conclusions

In the present study, the mechanical response of breast benign and malignant tumors was studied using a ramp-relaxation test on in vitro tissue specimens. The experimental data were interpolated by the KVFD model with three distinct parameters. These parameters were estimated for each sample through an accurate fitting of the practical test data.

It was found that, in general, the elastic parameter in malignant tumor tissue is higher than in benign tumor, and this is because of the higher density of cells in malignant tissue compared to benign one; thus, the tissue resistance to force increases. In some benign samples, ducts and connective tissue were formed, which created a space within the tissue and reduced the tissue's resistance to force. However, in some benign cases, it was seen that $E_0$is higher in malignant tissue, which was due to the presence of severe fibrosis in the breast tissue, which caused an enhanced tissue stiffness and resistance to force.

In comparing the fluidity parameter in benign and malignant tissues, it was found that, generally, α is higher in benign samples than in malignant tumors. These differences in two parameters of α and E_0, which are mechanical properties of the tissue, generally occur due to changes in the morphology and structure of cells and tissue that affect the cell density and type of cells.

Eventually, three malignant tumor tissues were examined together at different loading rates, and conspicuous differences were observed in the KVFD parameters. It was inferred that these differences depend on the cell density, the type of tissue-forming cells, the aggressiveness of malignant cells, and the malignant stage of cancerous tissue. The results of the present study can provide good insight for physicians to evaluate the type of tumors based on their mechanical response. These results also have good potential to distinguish between benign and malignant tumors without sample biopsy in future studies and research.

References

[1] D. Kashyap, D. Pal, R. Sharma, V. K. Garg, N. Goel, D. Koundal, A. Zaguia, S. Koundal, and A. Belay "Global Increase in Breast Cancer Incidence: Risk Factors and Preventive Measures," *BioMed Research International*, Vol. 2022, 2022, doi: https://doi.org/10.1155/2022/9605439.

[2] A. I. Riggio, K. E. Varley, and A. L. Welm, "The Lingering Mysteries of Metastatic Recurrence in Breast Cancer," *British Journal of Cancer*, Vol. 124, No. 1, pp. 13-26, 2021, doi: https://doi.org/10.1038/s41416-020-01161-4.

[3] A. Weber, M. d. Vivanco, and J. L. Toca-Herrera, "Application of Self-organizing Maps to AFM-based Viscoelastic Characterization of Breast Cancer Cell Mechanics," *Scientific Reports*, Vol. 13, No. 1, p. 3087, 2023, doi: https://doi.org/10.1038/s41598-023-30156-3.

[4] S. S. Abu-Naser and B. G. Bastami, "A Proposed Rule Based System for Breasts Cancer Diagnosis," *World Wide Journal of Multidisciplinary Research and Development*, pp. 27-33, 2016, [Online], Available: https://wwjmrd.com/upload/a-proposed-rule-based-system-for-breasts--cancer-diagnosis-.pdf.

[5] E. Pasquier, J. Rosendahl, A. Solberg, A. Ståhlberg, J. Håkansson, and G. Chinga-Carrasco, "Polysaccharides and Structural Proteins as Components in Three-dimensional Scaffolds for Breast Cancer Tissue Models: A Review," *Bioengineering*, Vol. 10, No. 6, p. 682, 2023, doi: https://doi.org/10.3390/bioengineering10060682.

[6] https://www.who.int/news-room/fact-sheets/detail/breast-cancer (accessed).

[7] L. Wilkinson and T. Gathani, "Understanding Breast Cancer as a Global Health Concern," *The British Journal of Radiology*, Vol. 95, No. 1130, p. 20211033, 2022, doi: https://doi.org/10.1259/bjr.20211033.

[8] A. Monshizadeh and A. Mojra, "Viscoelastic Analysis of Malignant Breast Tumors using Fractional Derivative Model Based on in Vitro Test Data," Presented at *the 31st Annual Conference Between Iran Mechanical Engineering and the 9th Iran Power Plant Industry*, 1402, [Online], Available: https://civilica.com/doc/1668617.

[9] G. N. Sharma, R. Dave, J. Sanadya, P. Sharma, and K. Sharma, "Various Types and Management of Breast Cancer: An Overview," *Journal of Advanced Pharmaceutical Technology & Research*, Vol. 1, No. 2, pp. 109-126, 2010, [Online], Available: https://journals.lww.com/japtr/fulltext/2010/01020/various_types_and_management_of_breast_cancer__an.3.aspx.

[10] K. Van Baelen, T. Geukens, M. Maetens, V. Tjan-Heijnen, C.J. Lord, S. Linn, F.-C. Bidard, F. Richard, W.W. Yang, R.E. Steele, S.J. Pettitt, C. Van Ongeval, M. De Schepper, E. Isnaldi, I. Nevelsteen, A. Smeets, K. Punie, L. Voorwerk, H. Wildiers, G. Floris, A. Vincent-Salomon, P.W.B. Derksen, P. Neven, E. Senkus, E. Sawyer, M. Kok, and C. Desmedt "Current and Future Diagnostic and Treatment Strategies for Patients with Invasive Lobular Breast Cancer," *Annals of Oncology*, Vol. 33, No. 8, pp. 769-785, 2022, doi: https://doi.org/10.1016/j.annonc.2022.05.006.

[11] A. Mojra and K. Hooman, "Viscoelastic Parameters of Invasive Breast Cancer in Correlation with Porous Structure and Elemental Analysis Data," *Computer Methods and Programs in Biomedicine,* Vol. 212, p. 106482, 2021, doi: https://doi.org/10.1016/j.cmpb.2021.106482.

[12] L. Wang, "Early Diagnosis of Breast Cancer," *Sensors*, Vol. 17, No. 7, p. 1572, 2017, doi: https://doi.org/10.3390/s17071572.

[13] R. Beňačka, D. Szabóová, Z. Guľašová, Z. Hertelyová, and J. Radoňák, "Classic and New Markers in Diagnostics and Classification of Breast Cancer," *Cancers,* Vol. 14, No. 21, p. 5444, 2022, doi: https://doi.org/10.3390/cancers14215444.

[14] K. K. Dwivedi, P. Lakhani, S. Kumar, and N. Kumar, "A Hyperelastic Model to Capture the Mechanical Behaviour and Histological Aspects of the Soft Tissues," *Journal of the Mechanical Behavior of Biomedical Materials,* Vol. 126, p. 105013, 2022, doi: https://doi.org/10.1016/j.jmbbm.2021.105013.

[15] A. Tecse, S. E. Romero, C. Romero, R. Naemi, and B. Castaneda, "Mechanical Validation of Viscoelastic Parameters for Different Interface Pressures using the Kelvin-Voigt Fractional Derivative Model," in *2022 44th Annual International Conference of the IEEE Engineering in Medicine & Biology Society (EMBC)*, 2022: IEEE, Glasgow, Scotland, United Kingdom, pp. 1512-1515, doi: https://doi.org/10.1109/EMBC48229.2022.9872009.

[16] S. Qiu, X. Zhao, J. Chen, J. Zeng, S. Chen, L. Chen, Y. Meng, B. Liu, H. Shan, M. Gao, and Y. Feng "Characterizing Viscoelastic Properties of Breast Cancer Tissue in a Mouse Model using Indentation," *Journal of Biomechanics,* Vol. 69, pp. 81-89, 2018, doi: https://doi.org/10.1016/j.jbiomech.2018.01.007.

[17] S. Dempsey and A. Samani, "Mechanical Properties of Breast Tissue," in *Biomechanics of the Female Reproductive System: Breast and Pelvic Organs*: Elsevier, pp. 169-207, 2023, doi:10.1016/b978-0-12-823403-7.00019-1.

[18] A. M. Teixeira and P. Martins, "A Review of Bioengineering Techniques Applied to Breast Tissue: Mechanical Properties, Tissue Engineering and Finite Element Analysis," *Frontiers in Bioengineering and Biotechnology,* Vol. 11, p. 1161815, 2023, doi: https://doi.org/10.3389/fbioe.2023.1161815.

[19] N. G. Ramiao, P. S. Martins, R. Rynkevic, A. A. Fernandes, M. Barroso, and D. C. Santos, "Biomechanical Properties of Breast Tissue, a State-of-the-art Review," *Biomechanics and Modeling in Mechanobiology,* Vol. 15, pp. 1307-1323, 2016, doi: https://doi.org/10.1007/s10237-016-0763-8.

[20] A. Tecse, S. E. Romero, R. Naemi, and B. Castaneda, "Characterisation of the Soft Tissue Viscous and Elastic Properties using Ultrasound Elastography and Rheological Models: Validation and Applications in Plantar Soft Tissue Assessment," *Physics in Medicine & Biology,* Vol. 68, No. 10, p. 105005, 2023, doi: 10.1088/1361-6560/acc923.

[21] H. Zhang, Y. Guo, Y. Zhou, H. Zhu, P. Wu, K. Wang, L. Ruan, M. Wan and M. F. Insana "Fluidity and Elasticity Form a Concise Set of Viscoelastic Biomarkers for Breast Cancer Diagnosis Based on Kelvin–Voigt Fractional Derivative Modeling," *Biomechanics and Modeling in Mechanobiology,* Vol. 19, No. 6, pp. 2163-2177, 2020, doi: https://doi.org/10.1007/s10237-020-01330-7.

[22] Y. Zhou, Y. Song, Z. Liu, W. Li, Y. Guo, L.A. Matkovic, X. Yang, R. Ma, M. Wan, L. Ruan, and H. Zhang "The Viscoelastic Characteristics of In-vitro Carotid Plaque by Kelvin-Voigt Fractional Derivative Modeling," *Journal of Biomechanics,* Vol. 141, p. 111210, 2022, doi: https://doi.org/10.1016/j.jbiomech.2022.111210.

[23] H. Zhang, Y. Wang, and M. F. Insana, "Ramp-hold Relaxation Solutions for the KVFD Model Applied to Soft Viscoelastic Media," *Measurement Science and Technology,* Vol. 27, No. 2, p. 025702, 2016, doi: 10.1088/0957-0233/27/2/025702.

[24] T. Ezenwafor, V. Anye, J. Madukwe, S. Amin, J. Obayemi, O. Odusanya, and W. Soboyejo "Nanoindentation Study of the Viscoelastic Properties of Human Triple Negative Breast Cancer Tissues: Implications for Mechanical Biomarkers," *Acta Biomaterialia,* Vol. 158, pp. 374-392, 2023, doi: https://doi.org/10.1016/j.actbio.2023.01.011.

[25] L. Ovalle-Flores, M. Rodríguez-Nieto, D. Zárate-Triviño, C. Rodríguez-Padilla, and J. L. Menchaca, "Methodologies and Models for Measuring Viscoelastic Properties of Cancer Cells: Towards a Universal Classification," *Journal of the Mechanical Behavior of Biomedical Materials,* Vol. 140, p. 105734, 2023, doi: https://doi.org/10.1016/j.jmbbm.2023.105734.

[26] H. Helisaz, "An Investigation of Cancer Effect on Viscoelastic Properties of Prostate Gland via Quasi-linear Viscoelastic Model," PhD Thesis, University of British Columbia, Vancouver, 2022, doi:10.14288/1.0420751, http://hdl.handle.net/2429/82760.

[27] E. Cavalcanti, M. Scaramuzzi, and R. Armentano, "A New Reliable Method for Tissue Preservation," *Pathology - Research and Practice,* Vol. 234, p. 153910, 2022, doi: https://doi.org/10.1016/j.prp.2022.153910.

[28] H. Zhang, Y. Wang, M. Fatemi, and M. F. Insana, "Assessing Composition and Structure of Soft Biphasic Media from Kelvin–Voigt Fractional Derivative Model Parameters4," *Measurement Science and Technology,* Vol. 28, No. 3, p. 035703, 2017, doi: 10.1088/1361-6501/aa5531.

[29] S. S. Poul, J. Ormachea, R. G. Gary, and K. J. Parker, "Comprehensive Experimental Assessments of Rheological Models' Performance in Elastography of Soft Tissues," *Acta Biomaterialia,* Vol. 146, pp. 259-273, 2022, doi: https://doi.org/10.1016/j.actbio.2022.04.047.

[30] J. Hu, Y. Zhou, J. D. Obayemi, J. Du, and W. O. Soboyejo, "An Investigation of the Viscoelastic Properties and the Actin Cytoskeletal Structure of Triple Negative Breast Cancer

Cells," *Journal of the Mechanical Behavior of Biomedical Materials,* Vol. 86, pp. 1-13, 2018, doi: https://doi.org/10.1016/j.jmbbm.2018.05.038.

[31] B. Carmichael, H. Babahosseini, S. Mahmoodi, and M. Agah, "The Fractional Viscoelastic Response of Human Breast Tissue Cells," *Physical Biology,* Vol. 12, No. 4, p. 046001, 2015, doi: 10.1088/1478-3975/12/4/046001.

[32] H. Zhang, Q. zhe Zhang, L. Ruan, J. Duan, M. Wan, and M. F. Insana, "Modeling Ramp-hold Indentation Measurements Based on Kelvin–Voigt Fractional Derivative Model," *Measurement Science and Technology,* Vol. 29, No. 3, p. 035701, 2018, doi: 10.1088/1361-6501/aa9daf.

Nomenclatures

English symbols

A	Cross-sectional area
E	Modulus of elasticity
$B(a: x. y)$	Incomplete beta function
$B(x. y)$	Complete beta function
G	Relaxation modulus
h_0	initial height
h(t)	Displacement
k	Speed of the indenter tip
P(t)	Force
R	Indenter radius
T_r	Ramp time

Greek symbols

α	Fluidity (real number)
$\Gamma(z)$	Gamma function
$\varepsilon(t)$	Strain
$\sigma(t)$	Stress
τ	Time constant
η	Viscous coefficient